J. Iron Steel Res. Int. (2023) 30:1613–1621
https://doi.org/10.1007/s42243-023-01023-2

ORIGINAL PAPER

Effect of stabilizing treatment on microstructure and stress rupture properties of phosphorus microalloyed Inconel 706 alloy

Sha Zhang[1,2] · Yu-chao Wu[3] · Yu Li[1] · Zhong-pei Dai[1] · Dan Jia[4] · Yan-fei Xu[1,2] · Guang-sheng Zeng[1,2] · Zhi-ming Guo[1,2] · Jian Liu[1,2]

Received: 1 February 2023 / Revised: 16 April 2023 / Accepted: 22 May 2023 / Published online: 30 June 2023

Abstract
The microstructure and stress rupture properties of Inconel 706 alloy microalloyed with phosphorus are examined under stabilizing and unstabilizing heat treatment conditions. It was found that applying the stabilizing treatment resulted in a 98% increment in the stress rupture life and a 215% increment in the elongation tested at 650 °C/690 MPa for the alloy compared to that under the unstabilizing heat treatment condition. The stabilizing treatment led to the precipitation of rod-shaped and needle-shaped η phases at the grain boundaries. Morphologies of γ′–γ″ co-precipitates in the grain interior were noncompact form and compact form for the alloy under unstabilizing and stabilizing heat treatment conditions, respectively. Based on the microstructure characterizations, the improvement of stress rupture properties by the stabilizing treatment was attributed to the precipitation of η phases at the grain boundaries, which can hinder cracks initiation and propagation and relieve the stress concentration.

Keywords Superalloy · Stabilization · η phase · γ′–γ″ co-precipitate · Stress rupture property

1 Introduction

Inconel 706 alloy is an age-hardenable Ni–Fe–Cr based superalloy. This alloy is used for various applications that require high mechanical strength combined with ease of fabrication, due to its low segregation tendency, good workability and machinability, and low cost [1–3]. In particular, the alloy is widely used for large forged gas turbine components [4–6]. The chemical composition of Inconel 706 alloy was derived from Inconel 718 alloy by removing Mo, reducing Ni, Cr, Nb, Al and C, and increasing Fe and Ti [1, 4]. The austenitic matrix of Inconel 706 alloy is strengthened by two different kinds of coherent, ordered compounds: the Ni_3Nb γ″ phase (tetragonal DO_{22} structure) and the $Ni_3(Al, Ti)$ γ′ phase (cubic $L1_2$ structure). The primary strengthening phase is γ″ phase, which is caused by coherency strains resulting from the large lattice misfit between the cubic cell of the γ matrix and the tetragonal cell of γ″ phase [2]. Moreover, a combined form of the two precipitates, a so-called "co-precipitate", can also form in Inconel 706 alloy, depending on the heat treatment and processing conditions. The morphologies of co-precipitates contain "compact" morphology (i.e., a cube-shaped γ′ particle coated on all six facets with a shell of γ″) and the "noncompact" morphology (where γ′ particle is sandwiched between two γ″ shells) [3, 7]. In addition to the main strengthening phases, the precipitation of η phases (DO_{24} structure) can effectively inhibit grain boundary sliding and enhance the resistance to the creep crack growth of Inconel 706 alloy [8–12].

✉ Sha Zhang
szhang10b@alum.imr.ac.cn

✉ Yan-fei Xu
yioffice123@126.com

1 College of Mechanical & Electrical Engineering, Changsha University, Changsha 410022, Hunan, China

2 Hunan Engineering Research Center of Research and Development of Degradable Materials and Molding Technology, Changsha University, Changsha 410022, Hunan, China

3 Changsha Kaiple Technology Co., Ltd., Changsha 410114, Hunan, China

4 Institute of Metal Research, Chinese Academy of Sciences, Shenyang 110016, Liaoning, China

Phosphorus (P) is one of the trace elements in primary raw materials for the production of superalloys [13]. Previous studies have shown that P increases the solidification temperature range and promotes the solidification segregation of elements in superalloys. Therefore, it has been suggested that the content of P should be decreased as low as possible to get superalloys with low segregation and excellent mechanical properties [14]. However, recently, researchers have found that microalloying with P can improve the creep properties and increase the stress rupture life of some wrought superalloys, such as Inconel 718, ATI 718Plus, and Inconel 706 alloys [15–23]. The beneficial effect of P is largely attributed to enhanced grain boundary cohesion and improved morphology and distribution of grain boundary precipitates, since P is found to be strongly segregated at grain boundaries.

It is necessary to further modify the chemical composition and optimize the heat treatment procedure of the superalloys for applications at even higher temperatures. As mentioned above, P microalloying is an effective way to increase the stress rupture properties of Inconel 706 alloy. Additionally, a stabilizing treatment between the solution and age hardening treatment has been proposed for the alloy to improve its creep rupture life [9, 10, 24]. However, the effect of stabilizing treatment on the microstructure and stress rupture properties of Inconel 706 alloy microalloyed with P is still unclear. Hence, in the present work, the effect of the stabilizing heat treatment on the microstructural evolutions and creep rupture properties of P microalloyed Inconel 706 alloy was investigated, which provides a basis for the development of Inconel 706 alloy with more excellent mechanical properties.

2 Experimental procedure

A P microalloyed Inconel 706 alloy with a higher stress rupture life compared with the standard alloy was manufactured in this study [19, 25]. The alloy ingot was vacuum induction melted with a mass of 10 kg. A homogenization treatment consisting of 1160 °C for 20 h and 1190 °C for 40 h was used to reduce residual elemental inhomogeneity. Following the homogenization, the ingot was forged, followed by hot rolling into bars of 16 mm in diameter. The starting temperature of forging and rolling was 1200 °C. The final temperature of forging and rolling was not lower than 950 °C. The chemical composition of the test alloy was Ni 41.93, Cr 15.36, Ti 1.82, Nb 2.64, Al 0.34, C 0.047, B 0.004, P 0.008 and Fe balance, in wt.%. Figure 1 shows

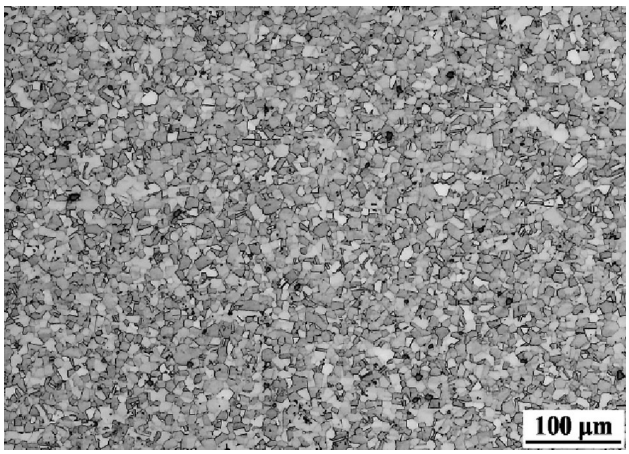

Fig. 1 Optical microscope image of as-rolled alloy

the as-rolled microstructure of the alloy. The average grain size was 11.5 ± 2.6 μm. The as-rolled samples were subjected to one of two heat treatments, and the corresponding schematic is presented in Fig. 2. In details, these two heat treatments were: (1) the unstabilizing heat treatment scheme including a solution treatment (980 °C for 3 h, air cooling) and a two-stage ageing treatment (730 °C/8 h, furnace cooling at 55 °C/h to 620 °C, holding for 8 h, air cooling), and (2) the stabilizing heat treatment scheme that added a stabilization treatment (845 °C for 3 h, air cooling) between the solution and ageing treatments.

After the heat treatments, the samples were machined into stress rupture samples with a 5-mm gauge diameter and a 25-mm gauge length. The stress rupture tests were performed at 650 °C/690 MPa until fracture. Two samples for each heat treatment were tested, and the average value was used to evaluate the stress rupture life and elongation.

The samples for optical microscope (OM, ZEISS Axiolab 5) and scanning electron microscope (SEM, TESCAN MIRA) observation were prepared by the standard metallographic method. The average sizes of grains and γ'' phases were measured by the linear intercept method. The samples were chemically etched using a solution of 5 g $CuCl_2$, 100 mL C_2H_5OH, and 100 mL HCl. The samples for transmission electron microscope (TEM, FEI Tecnai F30) observation were mechanically ground to a thickness of 50–60 μm with SiC papers, punched to a diameter of 3 mm, and then twin-jet electropolished in an electrolyte of 10 vol.% perchloric acid in methanol with a voltage of 24 V and –20 °C. The SEM equipped with an energy dispersive spectroscope (EDS) and TEM fitted with a high angle annular dark field (HAADF) detector were utilized for elemental analysis.

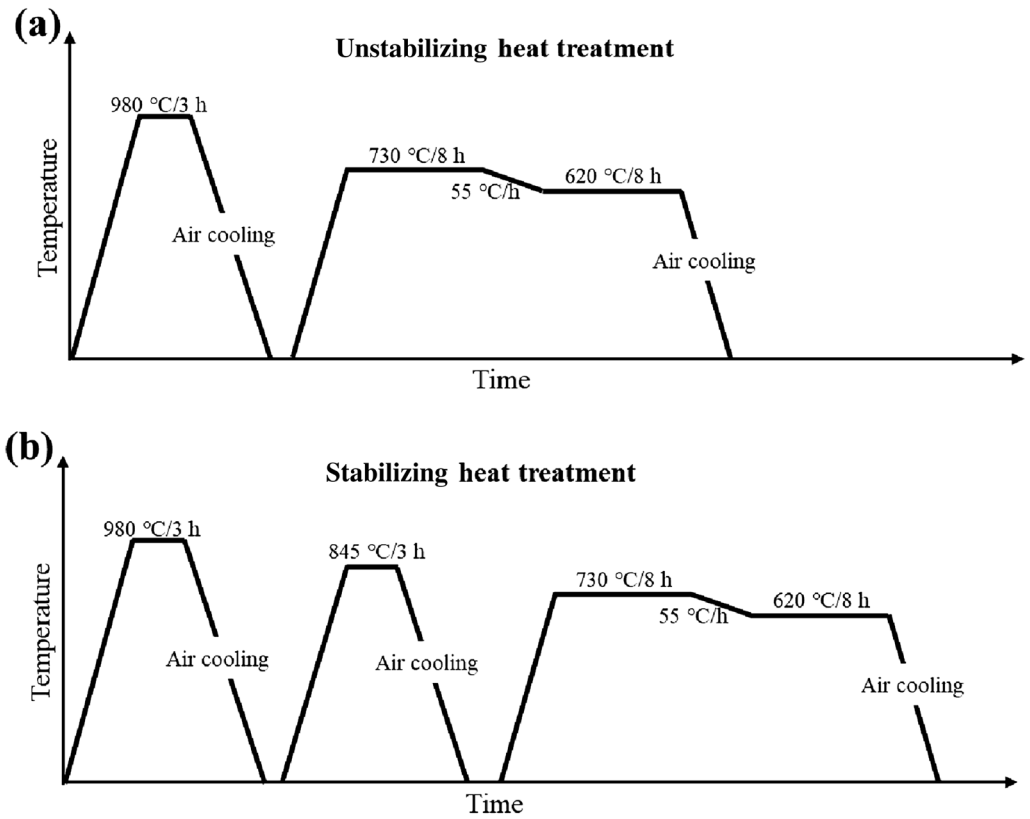

Fig. 2 Schematic of unstabilizing heat treatment (**a**) and stabilizing heat treatment (**b**)

3 Results

3.1 Microstructure

Figure 3 shows the microstructure of the as-rolled alloy after solution treatment at 980 °C for 3 h. The grain size of the sample was 46.6 ± 18.4 μm. Grain boundaries were free from precipitates, while a few grey-colored and white-colored particles were observed in γ matrix. The EDS point analysis indicated that the precipitates were Nb-rich MC carbides (Fig. 3b and c) [5].

The microstructures of the heat-treated samples are illustrated in Fig. 4. There was no precipitate at the grain boundaries of the unstabilized sample (Fig. 4a). In contrast, a number of intergranular precipitates were observed in the stabilized sample (Fig. 4b). TEM analysis was applied to identify the precipitates. Figure 5 shows the dark-field image and corresponding selected area electron diffraction (SAED) patterns of the precipitates at the grain boundary. The precipitates were found to be consistent with the close-packed hexagonal η phase [4, 26]. In the stabilized sample, the η phase appeared rod-shaped (Fig. 4c) or needle-shaped (Fig. 4d) at the grain boundaries. Additionally, γ″ and γ′ phase precipitated-free zone appeared around η phases, as shown in Fig. 4d [27, 28].

Figure 6 shows the HAADF image and associated chemical elements mapping around intergranular η phases in the stabilized sample. Compared with the matrix composition, the η phases were rich in Ni, Nb and Ti and poor in Fe and Cr. The element compositions of η phases in the present work are consistent with the previous studies [3, 29]. Although some studies have found that P atoms are segregated at interfaces of η/γ phases by atomic probe technique, this phenomenon was not found in this study, which may be due to the low content of P in the alloy and the inadequate resolution of TEM compared with atomic probe technique [30].

The intragranular microstructures observed by TEM are presented in Fig. 7. The presence of γ″ and γ′ precipitates in dark-field TEM images was confirmed, which was also indicated by the [001] zone axis diffraction patterns (inserted in Fig. 7). For the unstabilized sample, a few non-compact γ′–γ″ co-precipitates presented as sandwich-like morphology were observed, as marked in Fig. 7a. For the stabilized sample, compact γ′–γ″ co-precipitates, with cube-shaped γ′ particle covered by disk-shaped γ″ particles, were precipitated, and the average diameter of γ″ phase was 23.7 ± 3.9 nm (Fig. 7b). The sizes of γ″ and γ′ phases in the unstabilized sample were smaller than those in the stabilized sample, and the average diameter of γ″

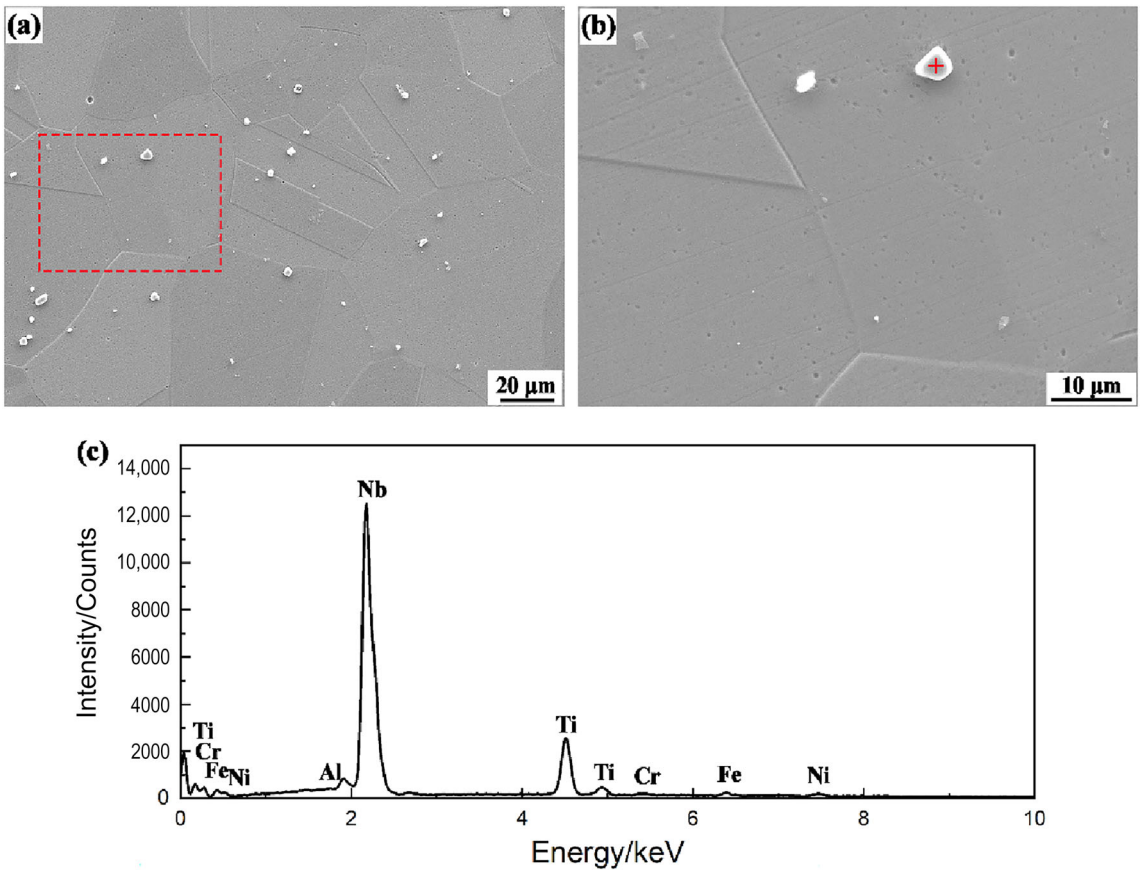

Fig. 3 Microstructure of alloy after solution treatment at 980 °C for 3 h. **a** SEM image; **b** high magnification SEM image of red dotted rectangle marked in **a**; **c** EDS spectrum of particles shown in **b**

phase was 15.0 ± 2.5 nm. Apparently, the size and distribution of intragranular precipitates were influenced by the stabilizing treatment.

3.2 Stress rupture properties

Figure 8 exhibits the stress rupture properties at 650 °C/690 MPa. The stress rupture life of the unstabilized sample was 59 h, while that of the stabilized sample was 117 h. The stabilizing treatment increased the stress rupture life of the alloy by 98%. The elongation was accordingly increased from 4.0% to 12.6%, with an increase in 215%. To clarify the fracture process of stress rupture tests, the fractured surfaces are displayed in Fig. 9. The fractured surfaces of the two heat-treated samples were composed of transgranular fracture zone and intergranular fracture zone (Fig. 9a, d). The intergranular fracture parts exhibited intergranular secondary cracks at the higher magnification SEM images, as marked by the yellow arrows in Fig. 9b, e. It is compared that more intergranular cracks were observed in the stabilized sample. The surface of grain boundaries in the intergranular fracture parts of the unstabilized sample was smooth without any deformation marks. In contrast, a few dimples existed on the fracture surfaces of the stabilized sample. With further detailed observation, the transgranular fracture parts of the two samples were detected under high magnification SEM images, showing that the sections were covered with dimples, as shown in Fig. 9c, f.

To reveal the intergranular cracks initiation and propagation during the stress rupture, the microstructures of the longitudinal sections near the fracture surface of the samples were observed by SEM, as shown in Fig. 10. It can be seen that there was no intergranular crack in the unstabilized sample except the secondary cracks near the main fracture cracks (Fig. 10a). By contrast, few intergranular cracks and holes in the interior of the stabilized sample were found (inserted in Fig. 10b).

4 Discussion

4.1 Effect of stabilizing treatment on microstructure

After the solution at 980 °C, the grains grew significantly (Fig. 3a). The stabilizing heat treatment scheme increased

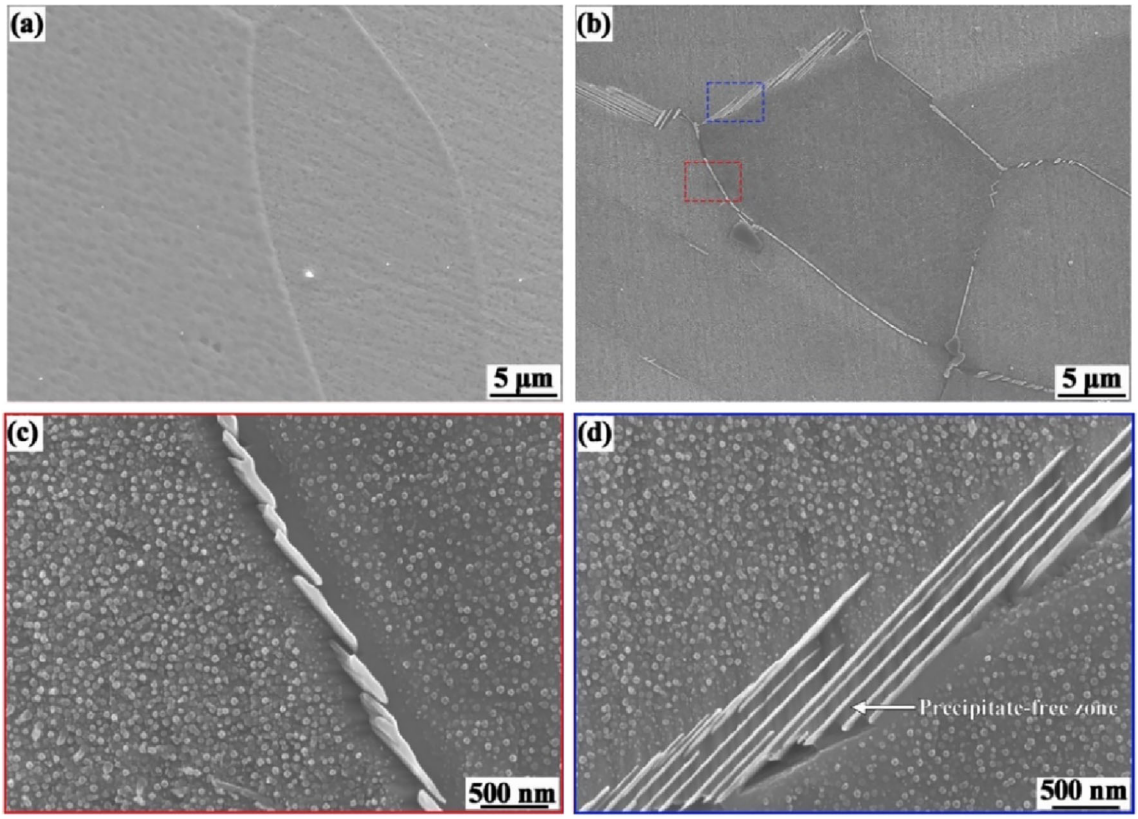

Fig. 4 SEM images of alloy under unstabilizing heat treatment (**a**) and stabilizing heat treatment (**b–d**) as well as high magnification image of red dotted rectangle (**c**) and blue dotted rectangle (**d**) in **b**

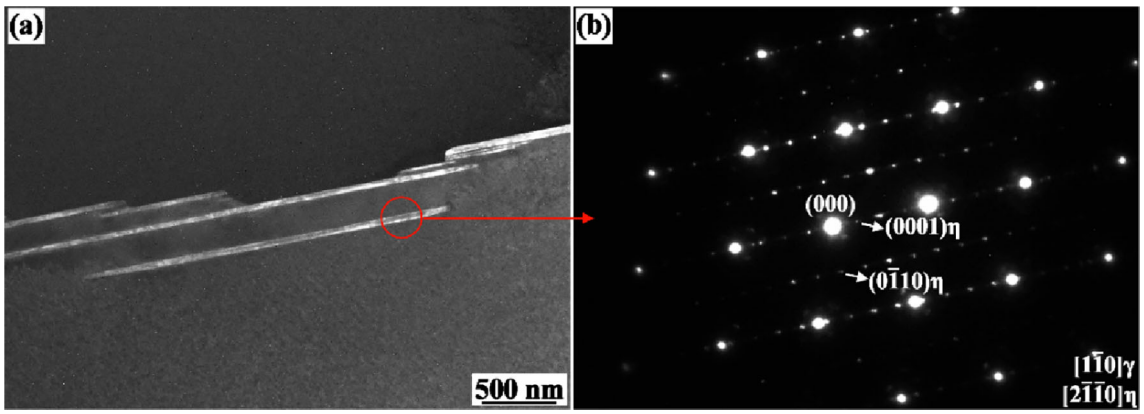

Fig. 5 TEM image of precipitated phase at grain boundary of alloy after stabilizing heat treatment. **a** Dark-field TEM image; **b** corresponding SAED patterns

the stabilizing treatment (845 °C/3 h) between the solution and ageing treatments in comparison with the unstabilizing heat treatment scheme. It is worth noticing that no grain growth occurred during the stabilizing treatment [31]. Therefore, the grain sizes were the same for the two heat-treated samples. The main difference in grain boundary microstructure between the samples was η phases precipitated in the stabilized sample, since the temperature of 845 °C crosses the η phase precipitation temperature range according to the time–temperature–transformation diagram [8]. In contrast, the sample that did not undergo the stabilizing treatment was free from intergranular η precipitates. The EDS mapping result shows that the η phases are rich in Ni, Nb and Ti, but poor in Fe and Cr, in comparison to the γ matrix. Therefore, the nucleation and growth of the η precipitates consume a certain amount of Ni, Nb and Ti in the γ matrix of the stabilized sample. As a result, the precipitation of γ″-Ni_3Nb and γ′-Ni_3(Al, Ti) phases during

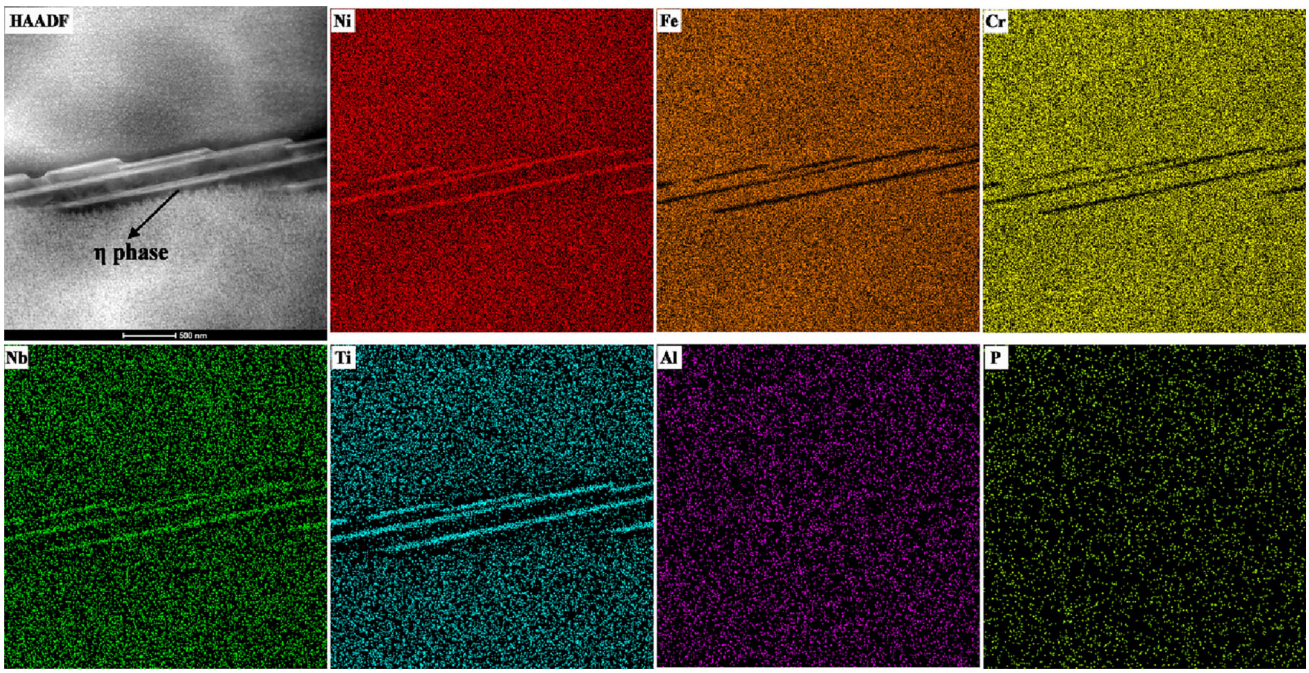

Fig. 6 HAADF image and associated EDS elemental mapping of whole area of alloy after stabilizing heat treatment

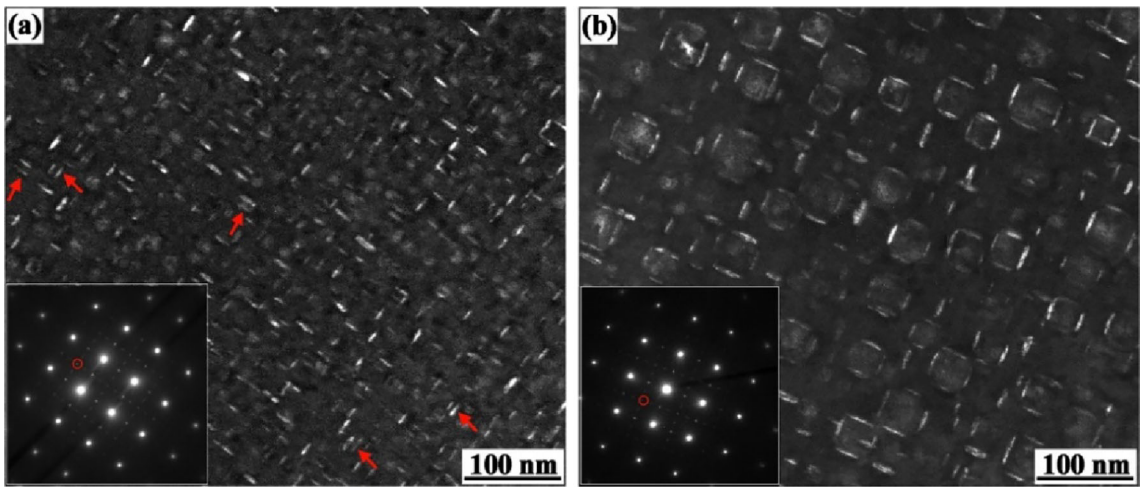

Fig. 7 Dark-field TEM images and corresponding SAED patterns of γ″ and γ′ phases in tested alloy. **a** Unstabilized sample; **b** stabilized sample

ageing treatment was impeded around η phases due to the lack of Ni, Nb and Ti, which caused the formation of the precipitate-free zone around η phases [4].

After the solution treatment (980 °C/3 h), the precipitates were dissolved completely except for carbides (Fig. 3), and the γ matrix is supersaturated solid solution. Based on the previous study, few disk-shaped γ″ and spherical γ′ phases are also precipitated in the stabilized sample during 845 °C besides the η phases [5]. The precipitation of η phases consumes a certain amount of Ni, Nb and Ti elements in the matrix. Thus, the supersaturation of the matrix is decreased after the stabilizing treatment carried out at 845 °C. After the two-stage ageing treatment (730 °C for 8 h, furnace cooling at 55 °C/h to 620 °C holding for 8 h, air cooling), new γ″ and γ′ precipitates were nucleated, and the pre-existing γ″ and γ′ precipitates grew. For the unstabilized sample, the high supersaturation of the matrix before ageing treatment leads to higher nucleation driving force of precipitates, compared to the stabilized sample. Thus, a large number of γ″ and γ′ precipitates are nucleated and competitively grown.

Cozar and Pineau [32] reported that the size of the initial γ′ particles before the formation of γ″ precipitates significantly affects the morphological characteristics of the γ′–γ″ co-precipitates in Inconel 718 alloy. If the initial size of the γ′ precipitate exceeds critical size (about 20 nm) during

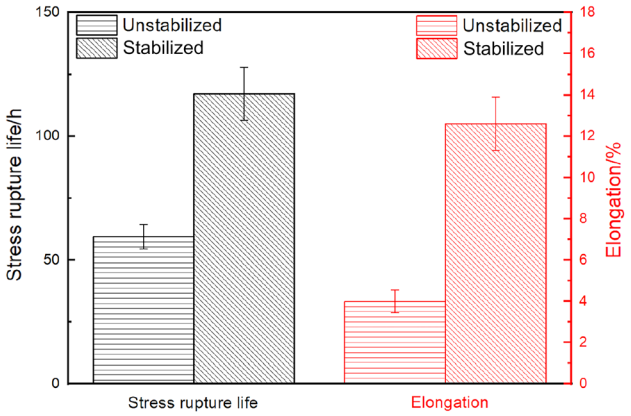

Fig. 8 Stress rupture properties of alloy under different heat treatment conditions

ageing, γ'' phase tends to precipitate on the six faces of the cube-shaped γ' particles. On the contrary, for the initial γ' particles smaller than the critical size, noncompact co-precipitates are obtained [32, 33]. Considering similar chemical composition with Inconel 718 alloy, it can be deduced that pre-existing γ' and low nucleation rate in the stabilized sample led to the γ'–γ'' co-precipitates appearing in compact morphology, while high nucleation rate caused noncompact morphology to appear in the unstabilized sample.

4.2 Mechanism of improvement in stress rupture properties by stabilizing treatment

From the fracture morphology (Fig. 9) and longitudinal section microstructure (Fig. 10), it could be known that the stress rupture cracks initiated from the grain boundaries and propagated along them during the stress loading. The applied stress was gradually increased with the propagation of the intergranular cracks, resulting in the transgranular fracture instantaneously [34]. Apparently, the heat treatment schemes did not change the fracture mode. Therefore, the influence of heat treatments on the stress rupture properties is closely relevant to the microstructure of grain boundaries. Accordingly, the difference in the intragranular microstructure between the samples under the two heat treatment conditions has little influence on the stress rupture properties in the present work.

In the process of polycrystalline plastic deformation, the grain boundaries hinder the movement of dislocations,

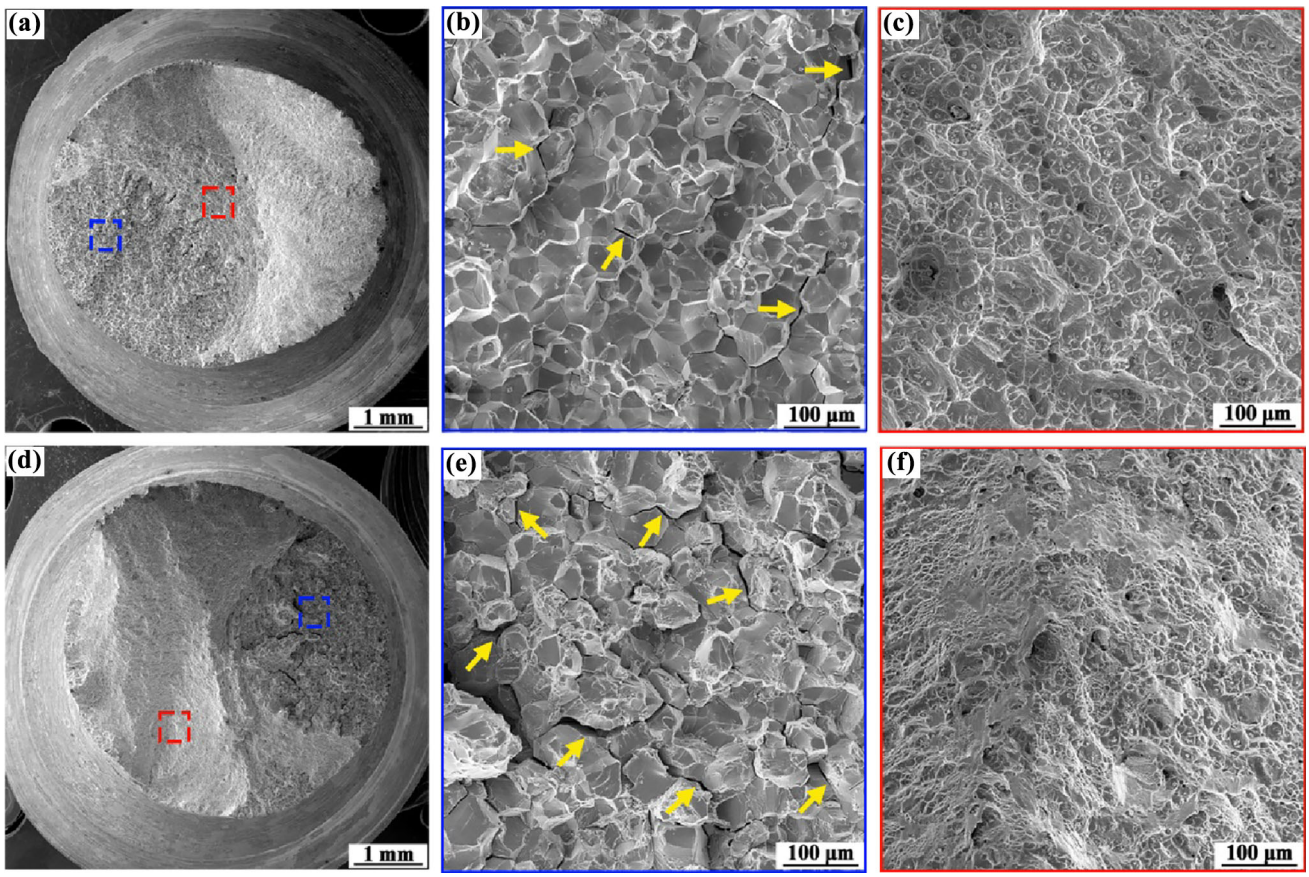

Fig. 9 Fractographs of alloy after stress rupture test. **a**–**c** Unstabilized sample; **d**–**f** stabilized sample. **b**, **c** are high magnification images in **a**; **e**, **f** are high magnification images in **d**

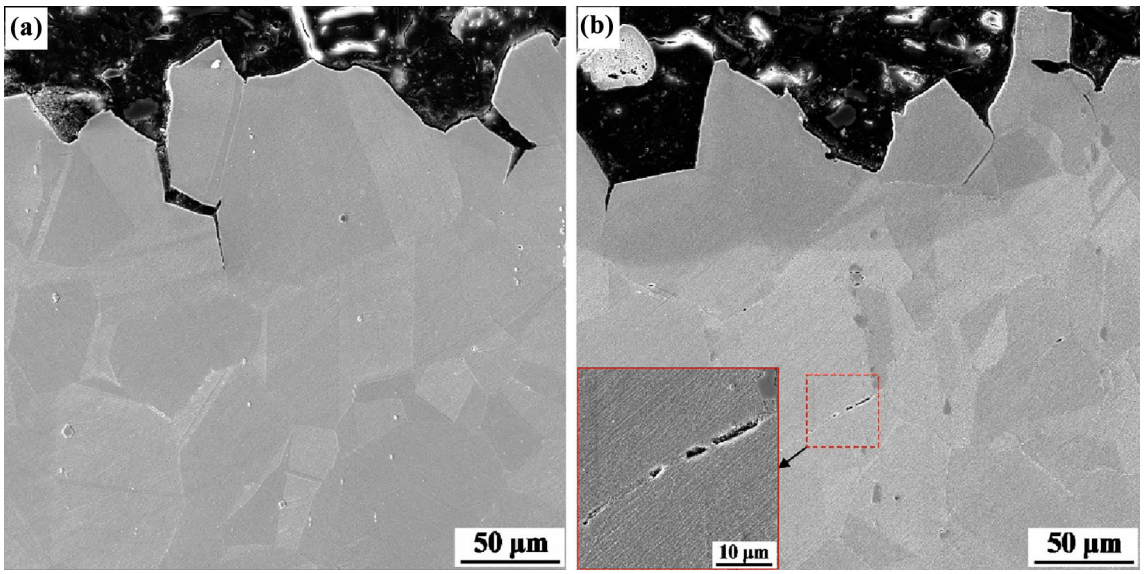

Fig. 10 Longitudinal microstructure of stress ruptured samples. **a** Unstabilized sample; **b** stabilized sample

which leads to the blockage of dislocations and stress concentration. The similar phenomenon is also reported in the high Mn and Al-containing steel [35]. Grain boundaries decorated with η phases in the stabilized sample can improve the stress rupture properties based on the mechanisms such as suppression of crack initiation and propagation, coordination of plastic deformation, and relief of stress concentration [9, 10, 36–38]. On the contrary, there was no η phase precipitated in the unstabilized sample. The initial cracks rapidly expand along the grain boundaries and lead to the final fracture. Consequently, there was no intergranular crack in the interior of the fractured sample except for the secondary crack near the main crack (Fig. 10a). It is deduced that the stabilized samples underwent a long loading period before fracture compared to the unstabilized samples. Therefore, more intergranular cracks were found in the longitudinal microstructures of the stress ruptured sample (Fig. 10b).

From the above discussion, the improvement in stress rupture properties of P microalloyed Inconel 706 alloy may be mainly due to the precipitation of η phases, which can hinder cracks initiation and propagation and relieve the stress concentration. Although it is found that the precipitation of η phases is significantly affected by the P addition, the beneficial effect of η phases was still effective in the present work [19].

5 Conclusions

1. After the unstabilizing heat treatment, the grain boundaries were free of η phases, and noncompact γ′–γ″ co-precipitates were formed in the grain interior. After the stabilizing heat treatment, the rod-shaped and needle-shaped η phases were distributed at the grain boundaries, and compact γ′–γ″ co-precipitates were formed in the grain interior.
2. The application of a stabilizing treatment at 845 °C resulted in a significant improvement in the stress rupture properties. The stress rupture life and elongation were increased by 98% and 215%, respectively. The stress rupture fracture was found to originate from the grain boundaries.
3. The precipitation of η precipitates at the grain boundaries after the stabilizing treatment can hinder cracks initiation and propagation and relieve the stress concentration, which may be beneficial for the rupture properties of P microalloyed Inconel 706 alloy.

Acknowledgements This work was supported by the National Natural Science Foundation of China (No. 52173034), the Science and Technology Innovation Program of Hunan Province of China (Nos. 2023JJ30081, 2022JJ40523 and 2021JJ50009), the Science Research Foundation of Hunan Provincial Education Department of China (No. 21A0546) and the Changsha Municipal Science and Technology Project (No. kq2203005).

Declarations

Conflict of interest The authors declare that they have no known competing financial interests or personal relationships that could have appeared to influence the work reported in this paper.

References

[1] P.W. Schilk, J.J. Pepe, R.C. Schwant, in: E.A. Loria (Eds.), Superalloys 718, 625, 706 and Various Derivatives, TMS, Warrendale, PA, USA, 1994, pp. 1–12.
[2] V. Kindrachuk, N. Wanderka, J. Banhart, D. Mukherji, D. Del Genovese, J. Rösler, Acta Mater. 56 (2008) 1609–1618.
[3] D. Mukherji, P. Strunz, D. Del Genovese, R. Gilles, J. Rosler, A. Wiedenmann, Metall. Mater. Trans. A 34 (2003) 2781–2792.
[4] T. Shibata, Y. Shudo, T. Takahashi, Y. Yoshino, T. Ishiguro, in: R.D. Kissinger, D.J. Wye, D.L. Anton, A.D. Cetel, M.V. Nathal, T.M. Pohck, D.A. Wcodford (Eds.), Superalloys 1996 (Eighth International Symposium), TMS, Warrendale, PA, USA, 1996, pp. 627–636.
[5] C. Kim, J. Park, H.U. Hong, J. Gu, Y. Song, J. Alloy. Compd. 900 (2022) 163479.
[6] P. Petit, J.P. Fesland, in: E.A. Loria (Eds.), Superalloys 718, 625, 706 and Various Derivatives, TMS, Warrendale, PA, USA, 1997, pp. 153–162.
[7] V. Kindrachuk, N. Wanderka, J. Banhart, Mater. Sci. Eng. A 417 (2006) 82–89.
[8] K.A. Heck, in: E.A. Loria (Eds.), Superalloys 718, 625, 706 and Various Derivatives, TMS, Warrendale, PA, USA, 1994 pp. 393–404.
[9] T. Takahashi, T. Ishiguro, K. Orita, J. Taira, T. Shibata, S. Nakata, in: E.A. Loria (Eds.), Superalloys 718, 625, 706 and Various Derivatives, TMS, Warrendale, PA, USA, 1994, pp. 557–565.
[10] J. Rösler, S. Müller, D. Del Genovese, M. Götting, in: E.A. Loria (Eds.), Superalloys 718, 625, 706 and Various Derivatives, TMS, Warrendale, PA, USA, 2001, pp. 523–534.
[11] O. Matsumoto, T. Honjo, Y. Yasumoto, T. Moriyama, T. Tsuchiyama, in: E.A. Loria (Eds.), Superalloys 718, 625, 706 and Various Derivatives, TMS, Warrendale, PA, USA, 1997, pp. 389–399.
[12] N. Wanderka, V. Naundorf, J. Banhart, D. Mukherji, D. Del Genovesse, J. Rösler, Surf. Interface Anal. 36 (2004) 546–551.
[13] A.V. Bromley, P.H. Parker, Metals Technol. 11 (1984) 419–427.
[14] Y.X. Zhu, S.N. Zhang, T.X. Zhang, J.H. Zhang, Z.Q. Hu, X.S. Xie, C.X. Shi, in: S.D. Antolovich, R.W. Stusrud, R.A. MacKay, D.L. Anton, T. Khan, R.D. Kissinger, D.L. Klarstrom (Eds.), Superalloys 1992, TMS, Warrendale, PA, USA, 1992, pp. 145–154.
[15] W.D. Cao, R.L. Kennedy, in: E.A. Loria (Eds.), Superalloys 718, 625, 706 and Various Derivatives, TMS, Warrendale, PA, USA, 1994, pp. 463–477.
[16] W.R. Sun, S.R. Guo, D.Z. Lu, Z.Q. Hu, Metall. Mater. Trans. A 28 (1997) 649–654.
[17] S. Guan, C. Cui, Y. Yuan, Y. Gu, Mater. Sci. Eng. A 662 (2016) 275–282.
[18] M. Wang, J. Du, Q. Deng, Z. Tian, J. Zhu, Mater. Sci. Eng. A 626 (2015) 382–389.
[19] S. Zhang, A. Zhang, L. Chang, W. Wang, X. Xin, W. Sun, Mater. Sci. Eng. A 761 (2019) 137981.
[20] C.S. Wang, Y.A. Guo, J.T. Guo, L.Z. Zhou, Mater. Des. 88 (2015) 790–798.
[21] Y. Wu, X. Qin, C. Wang, L. Zhou, Mater. Sci. Eng. A 768 (2019) 138454.
[22] Y. Wu, C. Wang, X. Qin, J. Hou, L. Zhou, J. Mater. Res. Technol. 18 (2022) 200–209.
[23] L. Li, Z. Liu, S. Tin, Metall. Mater. Trans. A 52 (2021) 2959–2972.
[24] G. Harkegard, W. Balbach, K. Stark, J. Rosler, in: E.A. Loria (Eds.), Superalloys 718, 625, 706 and Various Derivatives, TMS, Warrendale, PA, USA, 1997, pp. 425–430.
[25] S. Zhang, A. Zhang, C. Xue, D. Jia, W. Zhang, W. Wang, X. Xin, W. Sun, Crystals 10 (2020) 641.
[26] E.J. Pickering, H. Mathur, A. Bhowmik, O.M.D.M. Messé, J.S. Barnard, M.C. Hardy, R. Krakow, K. Loehnert, H.J. Stone, C.M.F. Rae, Acta Mater. 60 (2012) 2757–2769.
[27] B. Hassan, J. Corney, Mater. Sci. Technol. 33 (2017) 1879–1889.
[28] K. Hou, M. Ou, M. Wang, H. Li, Y. Ma, K. Liu, Mater. Sci. Eng. A 763 (2019) 138137.
[29] V. Kindrachuk, N. Wanderka, J. Banhart, D. Mukherji, D. Del Genovese, J. Rösler, Surf. Interface Anal. 39 (2007) 201–205.
[30] M. Wang, J.H. Du, Q. Deng, Z. Tian, J. Zhu, J. Alloy. Compd. 701 (2017) 635–644.
[31] S.V. Thamboo, in: E.A. Loria (Eds.), Superalloys 718, 625, 706 and Various Derivatives, TMS, Warrendale, PA, USA, 1997, pp. 211–217.
[32] R. Cozar, A. Pineau, Mater. Trans. 4 (1973) 47–59.
[33] D. Del Genovese, J. Rösler, P. Strunz, D. Mukherji, R. Gilles, Metall. Mater. Trans. A 36 (2005) 3439–3450.
[34] W.R. Sun, S.R. Guo, J.H. Lee, N.K. Park, Y.S. Yoo, S.J. Choe, Z.Q. Hu, Mater. Sci. Eng. A 247 (1998) 173–179.
[35] Z.B. Zheng, H.K. Yang, A.P. Shatrava, J. Long, Y.H. Wang, J.X. Li, K.H. Zheng, Mater. Sci. Eng. A 862 (2023) 144467.
[36] X. Li, J. Zhang, L. Rong, Y. Li, Mater. Sci. Eng. A 488 (2008) 547–553.
[37] W.J. Wan, G.W. Han, B. Deng, J. Iron Steel Res. Int. 17 (2010) No. 3, 67–71.
[38] M. Detrois, P.D. Jablonski, J.A. Hawk, Mater. Sci. Eng. A 799 (2021) 140337.